JOURNAL OF Materials CHEMISTRY

1,3-Diphenyl-5-(9-phenanthryl)-4,5-dihydro-1*H*-pyrazole (DPPhP): structure, properties, and application in organic light-emitting diodes

C. Q. Ma,[a] L. Q. Zhang,[a] J. H. Zhou,[a] X. S. Wang,*[a] B. W. Zhang,*[a] Y. Cao,[a] P. Bugnon,[b] M. Schaer,[b] F. Nüesch,[b] D. Q. Zhang[c] and Y. Qiu[c]

[a]*Technical Institute of Physics and Chemistry, Chinese Academy of Sciences, Beijing 100101, P. R. China. Tel: 86-10-6488-8103; Fax: 86-10-6488-6985; E-mail: g203@ipc.ac.cn*
[b]*Laboratoire d'Optoélectronique des Matériaux Moléculaires, Ecole Polytechnique Fédérale de Lausanne, EPFL, Lausanne, Switzerland,*
[c]*Department of Chemistry, Tsinghua University, Beijing 100084, P. R. China*

Received 20th August 2002, Accepted 22nd October 2002
First published as an Advance Article on the web 5th November 2002

A novel hole-transport material, 1,3-diphenyl-5-(9-phenanthryl)-4,5-dihydro-1*H*-pyrazole (DPPhP), was synthesized and fully characterized. The crystal structure of DPPhP was determined by X-ray diffraction analyses. DSC and AFM analysis demonstrate that DPPhP has a high T_g of 96 °C and good film forming ability. The hole-transport performance of DPPhP was examined by fabricating a multilayer device with structure of ITO/DPPhP (60 nm)/AlQ (60 nm)/LiF (0.8 nm)/Al, using DPPhP as the hole-transport layer along with an emitting-material, tris-(8-hydroxyquinolino)aluminium (AlQ). Both the brightness and efficiency of the device are about 30% higher than those of the device using *N,N′*-di-1-naphthenyl-*N,N′*-diphenyl-1,1′-biphenyl-4,4′-diamine (α-NPD) as the hole-transport layer.

Introduction

Organic light-emitting diodes (OLEDs) using small organic molecules have received considerable interest, after the initial work by Tang *et al.* in 1987,[1] because of the potential of using these devices as a low-cost alternative in lighting, back light, and flat panel displays. Much progress has been made recently in improving the efficiencies of electroluminescent (EL) devices by using multilayered structures,[2] doped emitting layers,[3] novel materials,[4] and efficient injection contacts.[5] One key to increasing the efficiency of an OLED device is to balance the charge carrier transport by adding a hole-transport layer and an electron-transport layer to the diode structure. The hole-transport layer in OLEDs provides efficient hole injection from the anode into the emitting layer and blocks electrons within this layer, in order to maximize the recombination probability of the injected carriers at the interface formed by the organic materials. Recently, many hole-transport materials (HTM) with high glass transition temperatures (T_g), predominantly based on the triarylamine functionality, including starburst amines,[6] spiro-linked amines,[7] and those with rigid groups,[8] have been investigated. Among these materials, *N,N′*-di-1-naphthenyl-*N,N′*-diphenyl-1,1′-biphenyl-4,4′-diamine (α-NPD)[9] is the most prevalent and has a high T_g of 98 °C. The high T_g prevents the HTM from recrystallization and thus improves the stability of OLEDs. 1,3,5-Triaryl-2-pyrazoline compounds have been used as hole-transporting materials in OLEDs for their good hole-transport ability, while most of them have low melting point and show poor thermal stability. Tano *et al.*[10] have demonstrated that pyrazoline dimers have higher melting points than pyrazoline monomers, and that stable amorphous films can be obtained by using these dimers. In our previous work,[11] we found that the introduction of condensed rings into the pyrazoline ring could increase the melting point of the compounds.

In the present work, we focus on the structure and properties of 1,3-diphenyl-5-(9-phenanthryl)-4,5-dihydro-1*H*-pyrazole (DPPhP), in which the phenanthryl group was introduced into the 5-position of the pyrazoline ring. X-ray diffraction analysis shows that DPPhP has a nonplanar structure, and that there is strong π stacking interaction in the solid state. This particular structure endues DPPhP with good film forming ability and a high T_g of 96 °C. Two EL devices with ITO/HTM/AlQ/LiF/Al structure were fabricated, where HTM was DPPhP and α-NPD, respectively. The comparison between the two OLEDs proved that DPPhP is an excellent hole-transport material for use in OLEDs.

Experimental section

General procedures

The structures of 1,3-diphenyl-4,5-dihydro-1*H*-pyrazole (DPP), 1,3-diphenyl-5-(9-phenanthryl)-4,5-dihydro-1*H*-pyrazole (DPPhP), *N,N′*-di-1-naphthenyl-*N,N′*-diphenyl-1,1′-biphenyl-4,4′-diamine (α-NPD), and tris(8-hydroxyquinolino)aluminium (AlQ) are shown in Chart 1. The synthetic step of DPPhP is shown in Scheme 1.[12] 9-Bromophenanthrene (**II**) and 9-phenanthrenealdehyde (**III**) were synthesized according to the literature, ref. 13 and ref. 14, respectively. ^{1}H NMR spectra were recorded on a Varian WM-300 (300 MHz), except for DPPhP which was measured on a Brüker DPX-400 (400 MHz). Mass spectra (MS) were measured on a Finnigan GC-MS 4021 C spectrophotometer. Elemental analysis was carried out on a Carlo Erba 1106 by the Flash EA 1112 method. The melting point of 9-phenanthrenealdehyde (**III**) and 3-(9-phenanthrenyl)-1-phenyl-2-propen-1-one (**VI**) were uncorrected. Infrared spectra of DPPhP were taken as KBr pellets using a Bio-Rad FTS-165 FT-IR spectrometer. Absorption and fluorescence spectra in solutions were recorded using a Shimadzu UV-1601PC UV–Vis spectrophotometer and a Hitachi F-4500 fluorescence spectrophotometer, respectively. The redox potentials were measured by cyclic voltammetry using a three electrode configuration on an EG&G Instruments Potentiostat/Galvanostat Model 283. The working electrode was a platinum wire, while a platinum wire and a saturated calomel electrode (SCE) served as counter and reference electrodes, respectively. A 0.1 M solution of Bu_4NBF_4 in acetonitrile was used as the supporting electrolyte and was flushed with N_2 previous to the measurements to avoid oxygen contamination.

DOI: 10.1039/b208130j

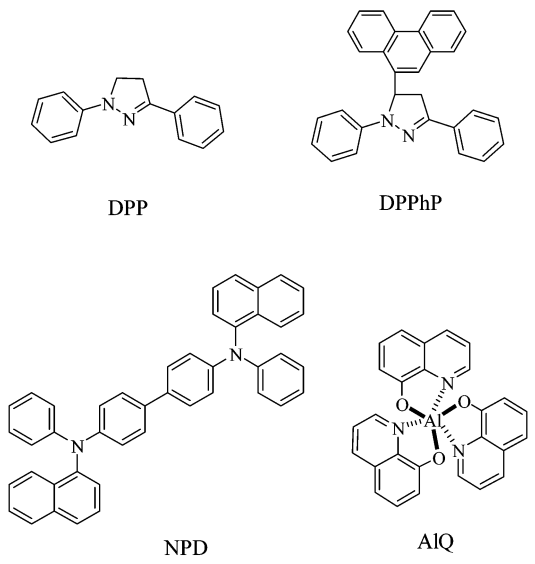

Chart 1 Molecular structures of DPP, DPPhP, α-NPD and AlQ.

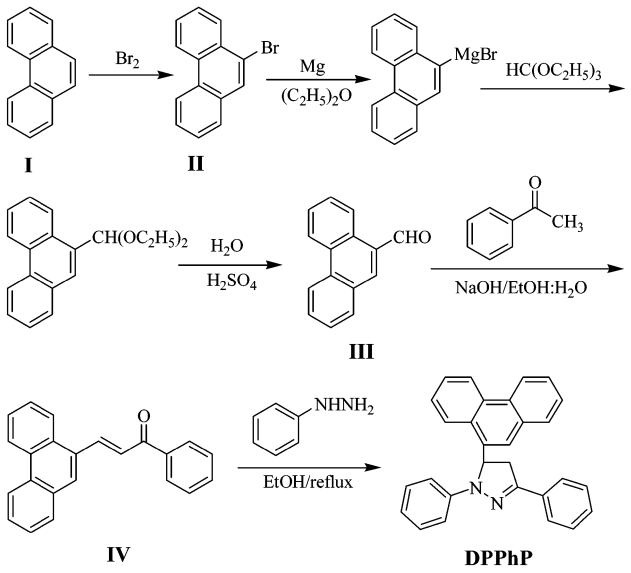

Scheme 1 Synthetic steps of DPPhP.

9-Phenanthrenealdehyde (III). m.p.: 99–100 °C, ^{1}H NMR: ($CDCl_3$, 300 MHz) δ: ppm 7.65–7.71 (t, 1H, J = 7.7 Hz), 7.73–7.79 (m, 2H), 7.79–7.86 (t, 1H, J = 7.5 Hz), 8.03–8.05 (d, 1H, J = 7.5 Hz), 8.25 (s, 1H), 8.68–-8.73 (t, 2H, J = 8.0 Hz), 9.36–9.40 (m, 1H), 10.38 (s, 1H).

3-(9-Phenanthrenyl)-1-phenyl-2-propen-1-one (VI). 9-Phenanthrenealdehyde (**III**, 8.3 g, 40 mmol) and acetophenone (5.0 g, 42 mmol) in 100 ml 95% EtOH were mixed with a solution of 100 ml 10% NaOH–EtOH + H_2O (2 : 1). The reaction mixture was stirred for 24 h at room temperature. The crystalline precipitate was filtered, washed with 95% EtOH and recrystallized from EtOH–H_2O to give 9.8 g (80%) yellow crystals. m.p.: 161–165 °C, ^{1}H NMR: ($CDCl_3$, 300 MHz) δ: ppm 7.54–7.75 (m, 8H), 7.96–7.98 (d, 1H, J = 7.6 Hz), 8.13–8.16 (m, 3H), 8.28–8.31 (d, 1H, J = 7.3 Hz), 8.66–8.69 (d, 1H, J = 8.0 Hz), 8.72 (s, 1H), 8.75–8.78 (d, 1H, J = 8.0 Hz).

1,3-Diphenyl-5-(9-phenanthrenyl)-2-pyrazoline (DPPhP). 3-(9-Phenanthrenyl)-1-phenyl-2-propen-l-one (**VI**, 4 g, 13 mmol) and phenylhydrazine (2.8 g, 26 mmol) were dissolved in 40 ml of EtOH. After refluxing for 10 h, the mixture was cooled to room temperature and the solid product was filtered and washed with EtOH to give 4.2 g of crude product. It was recrystallized from THF/EtOH to give the colorless DPPhP crystals (3.73 g, 72%). m.p.: 245–247 °C; T_g = 96 °C; ^{1}H NMR: ($CDCl_3$, 400 MHz) δ: 3.14–3.23 (m, 1H), 4.06–4.17 (q, J = 13.3 Hz, J = 15.7 Hz, 1H), 5.95–5.99 (m, 1H), 6.8 (t, J = 6.9 Hz, 1H), 7.12–7.21 (m, 5H); 7.32 (d, 1H, J = 7.2 Hz), 7.38 (t, 2H,
J = 7.6 Hz), 7.54 (t, 1H, J = 7.5 Hz), 7.63 (t, 1H, J = 7.1 Hz), 7.65–7.76 (m, 5H), 8.15–8.17 (m, 1H), 8.67 (d, 1H, J = 7.2 Hz), 8.82–8.85 (m, 1H); IR (KBR) v: 3050, 3025, 2898, 1597, 1505, 1490, 1399, 1338, 1143, 1051, 752, 724, 688 cm^{-1}; MS m/z (%): 398 (M^+, 33.68), 306 (21.97), 221 (30.13), 91 (100); elemental analysis calculated for $C_{29}H_{22}N_2$: C 87.41, H 5.56, N 7.03; found C 87.37, H 5.62, N 7.05.

X-ray crystallography analysis

The single crystal of DPPhP obtained from THF/EtOH solution was mounted on a brass pin, and the data were collected on a Rigakn R-Axis Rapid IP diffractometer with graphite-monochromated Mo Kα radiation operated at 50 kV and 300 mA at 25 °C over the 2θ range of 2.92–54.94°. No significant decay was observed during the data collection. Data were processed on a PC using the SHELXTL software package (version 5.0). The crystal belongs to a monoclinic space group, $P2_{1/n}$, uniquely determined by systematic absence; the structure was solved by direct methods. All non-hydrogen atoms were refined anistropically. The positions of hydrogen atoms were collated, and their contributions in structural factor calculation were included. The crystal data are summarized in Table 1. Selected bond lengths and angles are given in Table 2.

CCDC reference number 192205.

See http://www.rsc.org/suppdata/jm/b2/b208130j/ for crystallographic data in CIF or other electronic format.

Preparation of EL device and EL testing

EL devices fabricated in this work have the following configurations: device A, ITO/DPPhP (60 nm)/AlQ (60 nm)/LiF (0.8 nm)/Al; device B, ITO/NPD (60 nm)/AlQ (60 nm)/LiF (0.8 nm)/Al, where DPPhP and α-NPD were used as the hole-transport layer. AlQ was used as the emission layer. ITO-coated glass with a sheet resistance of 30 Ω per square was used

Table 1 Crystallographic data of DPPhP

Formula	$C_{29}H_{22}N_2$
Formula weight	398.49
Wavelength/Å	0.71073
Space group	$P2_{1/n}$
a/Å	8.3456 (4)
b/Å	9.1508 (3)
c/Å	27.9462 (14)
α	90°
β	91.735° (2)
γ	90°
Z	4
d_c/g·cm^{-1}	1.241
μ/cm^{-1}	0.72
$2\theta_{max}$	54.94°
No. of reflections measured	8146
No. of reflections used (R_{int})	4422 (0.0343)
No. of variables	281
Final R ($I > 2s(I)$)	
$R1^a$	0.0563
$wR2^b$	0.1342
R (all data)	
$R1$	0.1057
$wR2$	0.1554
Goodness of fit on F^2	1.022

$^a R1 = \Sigma|F_0|-|F_c|/\Sigma|F_0|$. $^b Rw2 = [\Sigma\omega[(F_0^2-F_c^2)^2]/\Sigma[\omega(F_0^2)^2]]^{1/2}$; $\omega = 1/[\sigma^2(F_0^2) + (0.075P)^2]$, where $P = [Max(F_0^2,0) + 2F_c^2]/3$.

Table 2 Selected bond lengths [Å], angles [degree], and torsion angles [degree] of DPPhP and DPP

	DPPhP	DPP[a]		DPPhP	DPP[a]
N(1)–N(2)	1.365(2)	1.336	N(1)–N(2)–C(21)	121.16(14)	121.0
N(2)–C(27)	1.466(2)	1.493	N(1)–N(2)–C(27)	112.82(15)	112.1
C(27)–C(28)	1.539(3)	1.521	C(21)–N(2)–C(27)	125.70(16)	126.8
C(28)–C(29)	1.502(3)	1.488	N(2)–C(27)–C(28)	101.63(15)	102.7
N(1)–C(29)	1.292(2)	1.333	C(27)–C(28)–C(29)	102.00(15)	102.4
C(21)–N(2)	1.388(2)	1.423	C(28)–C(29)–N(1)	112.97(17)	112.6
C(15)–C(29)	1.454(3)	1.408	C(28)–C(29)–C(15)	125.31 (17)	126.1
C(27)–C(14)	1.520(3)	—	N(1)–C(29)–C(15)	121.70(18)	120.7
			C(29)–N(1)–N(2)	109.16(15)	109.4
			C(14)–C(27)–C(28)	110.89(16)	—
			C(13)–C(14)–C(27)	121.84(16)	—
			C(16)–C(15)–C(29)	122.2(2)	—
			C(14)–C(27)–H(27A)	110.4	—

[a]From ref. 16.

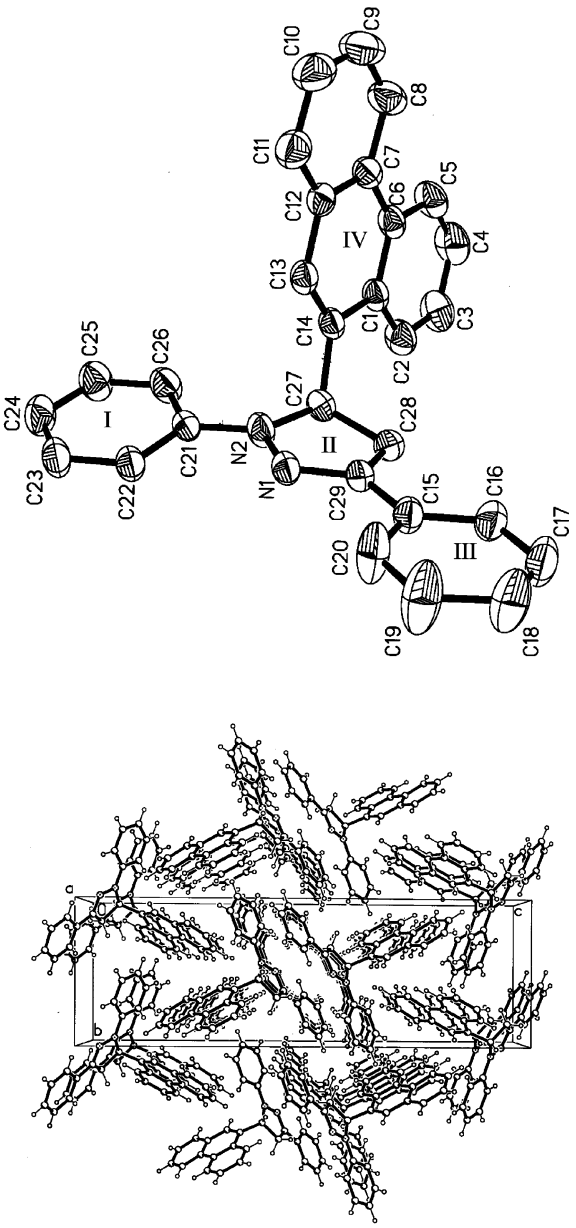

Fig. 1 Top: the molecular structure of DPPhP with labeling schemes and 50% thermal ellipsoids. Bottom: unit cell packing diagram of DPPhP.

as the substrate and anode. The substrates were first cleaned by ultrasonic agitation in organic solvents, followed by mechanical scrubbing in a non-ionic detergent. After further ultrasonication the substrates were thoroughly rinsed in ultra-pure water and dried. The substrates were then conveyed to a vacuum chamber for oxygen plasma cleaning. A plasma with a power of 10 W was generated using a magnetron for a duration of 4 min at a pressure of 0.1 torr. Subsequently, the organic films were vapor deposited at a base pressure of 10^{-7} torr. To enhance electron injection, a 0.8 nm thick LiF layer[15] was deposited onto AlQ. Electrical data were obtained with a Keithley 236 source-measure unit and light emission was collected with a calibrated photodiode. To calibrate the photodiode a Minolta L1-110 luminance meter was used to measure the light emission efficiency of the electroluminescent diode.

Table 3 The dihedral angles between planes

	Plane I	Plane II	Plane III
Plane II	14.3°		
Plane III	10.9°	4.7°	
Plane IV	86.1°	79.8°	84.0°

Results and discussion

Single crystal structure

In our previous work,[11] we found that the introduction of polycyclic aryl groups into the pyrazoline ring could increase the melting point of the pyrazoline derivatives. The significant increase of the melting point of pyrazoline derivatives is most likely caused by the changes in molecular weight and interactions in the solid state. Therefore, the crystal structure of DPPhP was measured by single-crystal X-ray diffraction analysis. As is shown in Fig. 1, DPPhP belongs to the space group $P2_{1/n}$. The selected interatomic bond lengths and bond angles are listed in Table 2, along with those of 1,3-diphenyl-4,5-dihydro-1*H*-pyrazole (DPP) given in the literature,[16] while the dihedral angles among planes are listed in Table 3. It can be seen that the two phenyl groups in DPPhP are conjugated with the pyrazoline ring and form a large conjugated π system, just like DPP. The dihedral angle between planes II and III for DPPhP is 4.7°, smaller than the value of 7.5° for DPP,[16] while the dihedral angle between planes II and I (14.3°) for DPPhP is larger by 8.9° than that of DPP (5.4°). These differences between the two molecules are probably due to the introduction of the sterically hindered phenanthryl group.

The bond angle of C(14)–C(27)–H(27A) of 110.4° and the dihedral angle between planes II and IV of 79.8° suggest that the phenanthryl group extends outside the pyrazoline ring. Therefore, the introduction of the bulky phenanthryl group decreases the symmetry of the compound and the resultant compound DPPhP has a nonplanar molecular structure. The nonplanar molecular structure can prevent regular packing of molecules and hence allows the formation of stable, amorphous DPPhP films.[17]

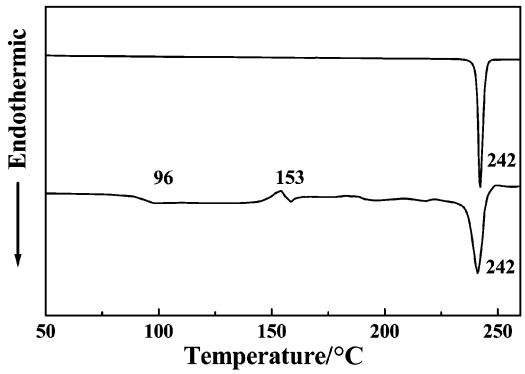

Fig. 2 DSC thermograms of DPPhP (heating rate, 10 °C min^{-1}).

The unit cell-packing diagram given in Fig. 1 (bottom) shows there is an extensive stacking between molecules of DPPhP in the crystal lattice. The distances of pyrazoline–pyrazoline and phenanthryl–phenanthryl are 3.50 Å and 3.06 Å, respectively. Compared with DPP, DPPhP has another π–π stacking interaction between two phenanthryl rings of two neighboring molecules. The relatively high molecular weight and intermolecular stacking in the solid state may account for the much higher melting point of DPPhP in comparison with that of DPP.

Thermal and morphologic behavior

Fig. 2 shows the DSC thermograms of DPPhP. When the crystalline sample of DPPhP is heated from room temperature, an endothermic peak due to the melting is observed at 242 °C. When the sample is rapidly cooled down with liquid nitrogen, it changes into an amorphous glassy state. When the amorphous glassy sample is again heated, an endothermic phenomenon is observed at 96 °C, at which the glassy state changes into the supercooled liquid state. Then a broad exothermic peak due to the crystallization is observed around 153 °C, followed by the endothermic peak due to the melting at 242 °C. This result shows that DPPhP has a high T_m of 242 °C and a high T_g of 96 °C. The high T_m and T_g are promising in view of the thermal stability of DPPhP films in EL devices.

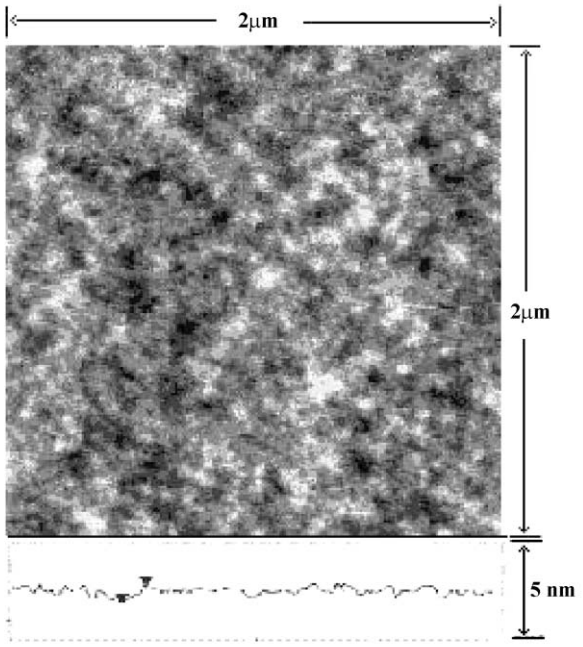

Fig. 3 The AFM micrograph revealing DPPhP film surface morphology.

Fig. 3 shows the surface morphology of the evaporated thin film of DPPhP observed by atomic force microscopy (AFM). The thin film was deposited on a cleaned indium tin oxide (ITO) glass substrate by vacuum deposition at 2×10^{-3} Pa. The deposition rate was about 0.3 nm s^{-1} and the thickness of the film is about 100 nm. Obviously the vapor deposited DPPhP film exhibits an entirely amorphous and flat surface with average roughness (R_a) about 0.37 nm. The good film forming ability and high glass transition temperature (T_g) of DPPhP could be due to its nonplanar molecular structure, as described above.

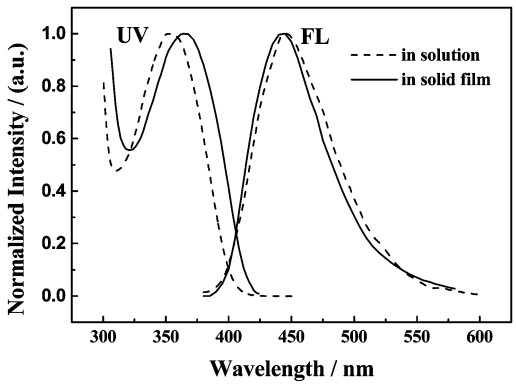

Fig. 4 UV-Vis and FL spectra of DPPhP in acetonitrile (5×10^{-6} M) and in solid film.

Optical properties

The absorption and photoluminescence (PL) spectra of DPPhP in acetonitrile (5×10^{-6} M) and in a solid film are shown in Fig. 4. The strong absorption bands around 360 nm both in solution and in the solid are quite similar to DPP,[18] which suggests that the introduction of bulky phenanthryl substitution on the pyrazoline ring does not appear to affect the ground state electronic structure of DPPhP. Similarly to DPP, DPPhP emits blue light at a wavelength around 440 nm both in acetonitrile solution and in the solid film, which means that the introduction of the phenanthryl group does not affect the excited state electronic structure of DPPhP either. Accordingly, the HOMO and LUMO remain almost unchanged in DPPhP and DPP, and the energy band gap of DPPhP was calculated to be 3.0 eV.

Redox properties and energy levels

Cyclic voltammetry[19] (CV) was used to study the redox properties of DPPhP and to estimate the HOMO and LUMO levels. As is shown in Fig. 5, the onset oxidation potential of

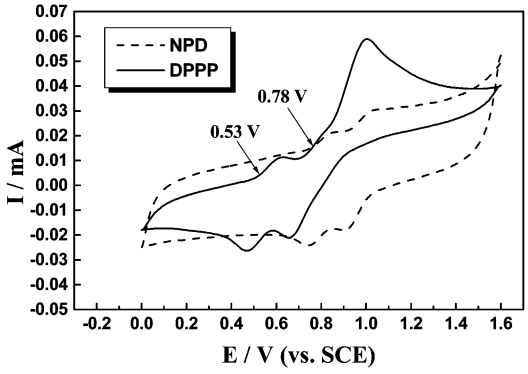

Fig. 5 Cyclic voltammogram of DPPhP and α-NPD in acetonitrile at a scan rate 400 mV s^{-1}.

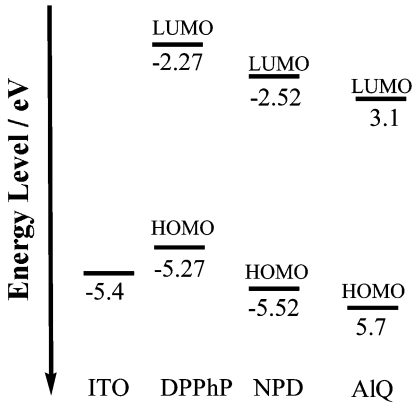

Fig. 6 Energy levels of electrodes and organic materials.

DPPhP was found to be 0.53 V at the Pt electrode *vs.* SCE in CH_3CN–Bu_4NBF_4 (0.1 M), while the value of α-NPD was found to be 0.78 V using the same conditions. According to the calculation by Noyes,[20] the NHE potential is taken to be −4.5 eV *vs.* vacuum. This leads to a potential of −4.74 eV *vs.* vacuum for the SCE. Consequently, the HOMO level is calculated as HOMO = $-(E_0^{ox} + 4.74)$ eV. Based on this equation, the HOMO energies of DPPhP and α-NPD are calculated to be −5.27 eV and −5.52 eV, respectively. The LUMO energy levels are obtained by subtraction of the optical band gap from the HOMO. The energy levels of electrodes and organic materials are shown in Fig. 6. Note that the work function of ITO is −5.4 eV due to oxygen plasma treatment.[21] From the low oxidation potential of DPPhP, it can be inferred that hole injection from ITO should be even more efficient than for α-NPD. Additionally, a rather important hole injection barrier of 0.43 eV is expected at the interface between DPPhP and AlQ. In view of the good film forming ability, high T_g and barrierless hole injection from the ITO anode, DPPhP is a very promising hole-transport material. As we demonstrate below, its charge transport properties are similar to those of α-NPD.

Electroluminescence

To study the EL performance of DPPhP, a multilayer diode structure composed of ITO–DPPhP (60 nm)/AlQ (60 nm)/LiF (0.8 nm)/Al (device A) was fabricated and compared to a reference device using α-NPD instead of DPPhP as hole-transport layer (device B). When the diodes were driven in forward bias, both devices emitted similar green light with a peak at around 540 nm, which is attributed to the emission of AlQ.[1] This suggests that DPPhP served as hole-transport layer in device A, similarly to α-NPD in device B.

Fig. 7 gives the current density–voltage (*J–V*) and brightness–current density (*L–J*) characteristics of the two EL devices. It appears that the current density is lower for device A, but its light output at a given current density is higher than for device B. Fig. 8 gives the plots of the external quantum efficiency *versus* driving voltage for both devices, from which

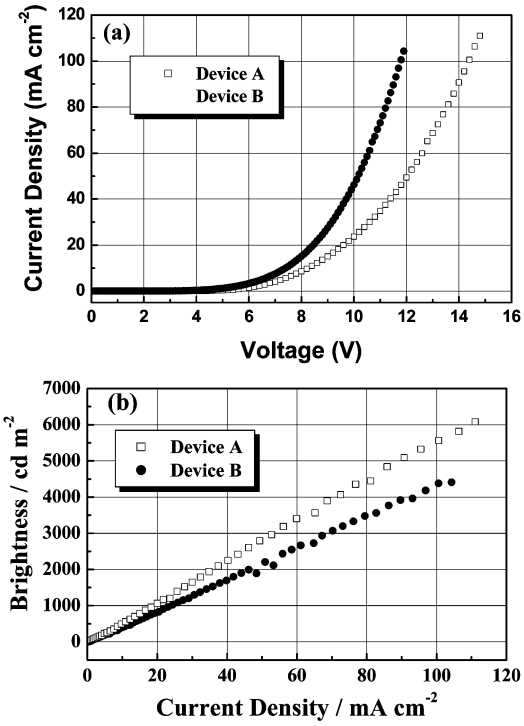

Fig. 7 *J–V* (a) and *L–J* (b) characteristics for devices A and B.

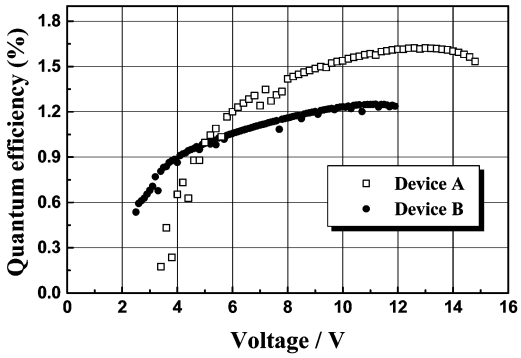

Fig. 8 External quantum efficiency as a function of bias voltage for devices A and B.

it can be clearly seen that EL device using DPPhP as hole-transport layer has higher external quantum efficiency than the device using α-NPD as hole-transport layer. The maximum external quantum efficiency of device A is 1.6% (5.5 cd A^{-1}, 60 mA cm^{-2}, 3402 cd m^{-2}, 12.6 V), compared to 1.2% (4.4 cd A^{-1}, 79 mA cm^{-2}, 3475 cd m^{-2}, 11.2 V) for device B. The performances for both devices at a current density of 20 mA cm^{-2} are summarized in Table 4, along with some published results of α-NPD/AlQ devices. Clearly, device A shows a 30% higher efficiency and brightness as compared to device B. We have attributed the high efficiency of devices using

Table 4 Property comparison of devices A and B at 20 mA cm^{-2} along with the published results of α-NPD/AlQ devices

Device	λ_{em}^{max}/nm	L/cd m^{-2}	External efficiency (%)	Power efficiency/lm W^{-1}	Reference
ITO/DPPhP (60 nm)/AlQ (60 nm)/LiF (0.8 nm)/Al	541	1066	1.52	1.71	This work
ITO/α-NPD (60 nm)/AlQ (60 nm)/LiF (0.8 nm)/Al	531	828	1.15	1.46	This work
ITO/α-NPD (40 nm)/AlQ (40 nm)/Mg–Ag (10 : 1)/Ag	518	—	0.6[a]	—	22
ITO/α-NPD/AlQ/Mg–Ag (10 : 1)	524	1140	—	—	23
ITO/SiO_2 (1.0 nm)/α-NPD/AlQ/Mg–Ag (10 : 1)	524	1892	—	—	23
ITO/α-NPD (40 nm)/AlQ (40 nm)/Mg–Ag (10 : 1)	520	2870[a]	1.07	1.42	24
ITO/α-NPD (60 nm)/AlQ (75nm)/ Mg–Ag (10 : 1)	—	950[b]	—	—	25

[a]At current density of 100 mA cm^{-2}. [b]At current density of 31.25 mA cm^{-2}.

DPPhP as HTM to a better hole confinement and more efficient recombination at the DPPhP/AlQ interface. The rather high energy barrier for holes at this interface could as well be responsible for the lower current densities observed in device A.

Conclusion

The introduction of phenanthryl group on 5-position of pyrazoline ring gives DPPhP with a nonplanar molecular structure, which can form uniform amorphous film with a high T_g of 96 °C. Moreover, the high HOMO energy level of DPPhP facilitates hole injection from ITO and the rather high energy barrier between DPPhP and AlQ confines the charge carriers at the DPPhP/AlQ interface. The EL device with ITO/DPPhP/AlQ/LiF/Al structure using DPPhP as hole-transport layer shows an external efficiency as high as 1.6%.

Acknowledgements

The authors would like to thank the NNSFC for financial support (No. 29971031, 20073050).

References

1 C. W. Tang and S. A. VanSlyke, *Appl. Phys. Lett.*, 1987, **51**, 913.
2 M. Ikai, S. Tokito, Y. Sakamoto, T. Suzuki and Y. Taga, *Appl. Phys. Lett.*, 2001, **79**, 156.
3 C. W. Tang, S. A. VanSlyke and C. H. Chen, *J. Appl. Phys.*, 1989, **65**, 3610.
4 Z. Shen, P. E. Burrows, V. Bulović, S. R. Forrest and M. E. Thompson, *Science (Washington, D. C.)*, 1997, **276**, 2009.
5 S. A. VanSlyke, C. H. Chen and C. W. Tang, *Appl. Phys. Lett.*, 1996, **69**, 2160.
6 M. Thelakkat and H.-W. Schmidt, *Adv. Mater.*, 1998, **10**, 219.
7 J. Salbeck and F. Weissortel, *Macromol. Symp.*, 1997, **125**, 121.
8 B. E. Koene, D. E. Loy and M. E. Thompson, *Chem. Mater.*, 1998, **10**, 2235.
9 C. H. Chen, J. Shi and C. W. Tang, *Macromol. Symp.*, 1997, **125**, 1.
10 T. Sano, T. Fujii, Y. Nishio, F. Hamada, K. Shibata and K. Kuroki, *Jpn. J. Appl. Phys.*, 1995, **34**, 3124.
11 C. Q. Ma, L. Q. Zhang, X. H. Li, X. S. Wang, B. W. Zhang, Y. Cao, D. M. Wang, X. Y. Jiang, Z. L. Zhang, D. Q. Zhang and Y. Qiu, *Acta Chim. Sinica*, 2002, **60**, 847.
12 E. R. Donnald, R. Judi and F. K. W. John, *Aust. J. Chem.*, 1979, **32**, 1601.
13 *Org. Synth. Coll. Vol.* 3, John Wiley & Sons, New York, 1963, p. 134.
14 *Org. Synth. Coll. Vol.* 3, John Wiley & Sons, New York, 1963, p. 701.
15 L. S. Hung, C. W. Tang and M. G. Mason, *Appl. Phys. Lett.*, 1997, **70**, 152.
16 B. Duffin, *Acta Cryst.*, 1968, **B24**, 1256.
17 Y. Shirota, *J. Mater. Chem.*, 2000, **10**, 1.
18 G. Q. Yang and S. K. Wu, *J. Photochem. Photobiol. A: Chem.*, 1992, **66**, 69.
19 A. K. Agrawal and S. A. Jenekhe, *Chem. Mater.*, 1996, **8**, 579.
20 R. M. Noyes, *J. Am. Chem. Soc.*, 1962, **39**, 309.
21 F. Nüesch, M. Carrara, M. Schaer, D. B. Romero and L. Zuppiroli, *Chem. Phys. Lett.*, 2001, **347**, 311.
22 D. E. Loy, B. E. Koene and M. E. Thompson, *Adv. Funct. Mater.*, 2002, **12**, 245.
23 Z. B. Deng, X. M. Ding, S. T. Lee and W. A. Gambling, *Appl. Phys. Lett.*, 1999, **74**, 2227.
24 C. W. Ko and Y. T. Tao, *Synth. Met.*, 2002, **126**, 37.
25 H. Aziz and A. D. Popovic, *Appl. Phys. Lett.*, 2002, **80**, 2227.